

Effects of synaptic and myelin plasticity on learning in a network of Kuramoto phase oscillators

Citation for published version (APA):

Karimian, M., Dibenedetto, D., Moerel, M., Burwick, T., Westra, R. L., De Weerd, P., & Senden, M. (2019). Effects of synaptic and myelin plasticity on learning in a network of Kuramoto phase oscillators. *Chaos*, 29(8), Article 083122. <https://doi.org/10.1063/1.5092786>

Document status and date:

Published: 01/08/2019

DOI:

[10.1063/1.5092786](https://doi.org/10.1063/1.5092786)

Document Version:

Publisher's PDF, also known as Version of record

Document license:

Taverne

Please check the document version of this publication:

- A submitted manuscript is the version of the article upon submission and before peer-review. There can be important differences between the submitted version and the official published version of record. People interested in the research are advised to contact the author for the final version of the publication, or visit the DOI to the publisher's website.
- The final author version and the galley proof are versions of the publication after peer review.
- The final published version features the final layout of the paper including the volume, issue and page numbers.

[Link to publication](#)

General rights

Copyright and moral rights for the publications made accessible in the public portal are retained by the authors and/or other copyright owners and it is a condition of accessing publications that users recognise and abide by the legal requirements associated with these rights.

- Users may download and print one copy of any publication from the public portal for the purpose of private study or research.
- You may not further distribute the material or use it for any profit-making activity or commercial gain
- You may freely distribute the URL identifying the publication in the public portal.

If the publication is distributed under the terms of Article 25fa of the Dutch Copyright Act, indicated by the "Taverne" license above, please follow below link for the End User Agreement:

www.umlib.nl/taverne-license

Take down policy

If you believe that this document breaches copyright please contact us at:

repository@maastrichtuniversity.nl

providing details and we will investigate your claim.

Effects of synaptic and myelin plasticity on learning in a network of Kuramoto phase oscillators

Cite as: Chaos 29, 083122 (2019); <https://doi.org/10.1063/1.5092786>

Submitted: 14 February 2019 • Accepted: 01 August 2019 • Published Online: 22 August 2019

 M. Karimian,  D. Dibenedetto,  M. Moerel, et al.



View Online



Export Citation



CrossMark

ARTICLES YOU MAY BE INTERESTED IN

[Erratum: “Effects of synaptic and myelin plasticity on learning in a network of Kuramoto phase oscillators” \[Chaos 29, 083122 \(2019\)\]](#)

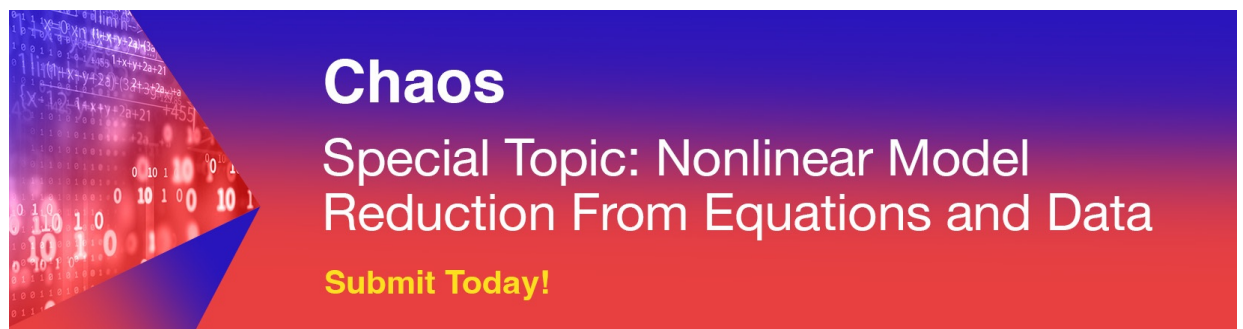
[Chaos: An Interdisciplinary Journal of Nonlinear Science 30, 069902 \(2020\); <https://doi.org/10.1063/5.0013005>](#)

[Low dimensional behavior of large systems of globally coupled oscillators](#)

[Chaos: An Interdisciplinary Journal of Nonlinear Science 18, 037113 \(2008\); <https://doi.org/10.1063/1.2930766>](#)

[Time-delayed Kuramoto model in the Watts–Strogatz small-world networks](#)

[Chaos: An Interdisciplinary Journal of Nonlinear Science 31, 113125 \(2021\); <https://doi.org/10.1063/5.0064022>](#)



Chaos
Special Topic: Nonlinear Model
Reduction From Equations and Data
Submit Today!

Effects of synaptic and myelin plasticity on learning in a network of Kuramoto phase oscillators

Cite as: Chaos 29, 083122 (2019); doi: 10.1063/1.5092786

Submitted: 14 February 2019 · Accepted: 1 August 2019 ·

Published Online: 22 August 2019



View Online



Export Citation



CrossMark

M. Karimian,¹  D. Dibenedetto,¹  M. Moerel,^{1,2,3}  T. Burwick,^{1,4}  R. L. Westra,^{1,5}  P. De Weerd,^{1,2,3}  and M. Senden^{2,3} 

AFFILIATIONS

¹Maastricht Centre for Systems Biology (MaCSBio), Maastricht University, 6229 ER Maastricht, The Netherlands

²Department of Cognitive Neuroscience, Faculty of Psychology and Neuroscience, Maastricht University, P.O. Box 616, 6200 MD Maastricht, The Netherlands

³Maastricht Brain Imaging Centre, Faculty of Psychology and Neuroscience, Maastricht University, P.O. Box 616, 6200 MD Maastricht, The Netherlands

⁴Frankfurt Institute for Advanced Studies, Goethe University Frankfurt, Ruth-Moufang-Str. 1, 60438 Frankfurt am Main, Germany

⁵Department of Data Science and Knowledge Engineering, Maastricht University, 6211 LH Maastricht, The Netherlands

ABSTRACT

Models of learning typically focus on synaptic plasticity. However, learning is the result of both synaptic and myelin plasticity. Specifically, synaptic changes often co-occur and interact with myelin changes, leading to complex dynamic interactions between these processes. Here, we investigate the implications of these interactions for the coupling behavior of a system of Kuramoto oscillators. To that end, we construct a fully connected, one-dimensional ring network of phase oscillators whose coupling strength (reflecting synaptic strength) as well as conduction velocity (reflecting myelination) are each regulated by a Hebbian learning rule. We evaluate the behavior of the system in terms of structural (pairwise connection strength and conduction velocity) and functional connectivity (local and global synchronization behavior). We find that adaptive myelination is able to both functionally decouple structurally connected oscillators as well as to functionally couple structurally disconnected oscillators. With regard to the latter, we find that for conditions in which a system limited to synaptic plasticity develops two distinct clusters both structurally and functionally, additional adaptive myelination allows for functional communication across these structural clusters. These results confirm that network states following learning may be different when myelin plasticity is considered in addition to synaptic plasticity, pointing toward the relevance of integrating both factors in computational models of learning.

Published under license by AIP Publishing. <https://doi.org/10.1063/1.5092786>

Synaptic and myelin plasticity are two crucial mechanisms underlying learning in the brain. Synaptic plasticity, which refers to activity-dependent changes of synaptic coupling, has been modeled intensely in recent decades. However, myelin plasticity, which refers to activity-dependent changes in the structure and thickness of myelin sheaths, has been largely absent from computational models of learning. These two plasticity mechanisms are likely to exhibit complex interactions. In this work, we suggest a simple mathematical framework as a first attempt to understand these interactions. Our results may pave the way for the development of new models of learning incorporating both synaptic and myelin plasticity.

I. INTRODUCTION

Synchronization, the mutual adjustment of rhythms among interacting oscillators,^{1,2} is a ubiquitous phenomenon in physics, biology, and neuroscience.^{3–6} In the latter, this phenomenon has been linked to various cognitive functions including perception,^{7–9} attention,^{10–14} and learning.^{15–25} Learning involves the dynamic adjustment of connections among neuronal populations in the form of synaptic plasticity.²⁶ Mutual interactions between synaptic plasticity and synchronization have been of particular interest in neuroscience.^{19–25,27–30} However, synaptic plasticity is not the only factor being affected by as well as affecting synchronized activity in oscillating neuronal populations. Myelination is also

activity-dependent,^{31–38} and since it influences the conduction velocity of neuronal signals, it is an additional dynamic factor potentially affecting synchronization behavior. Myelination is integral to the unimpaired functioning of the brain as it ensures that signals originating from presynaptic sources at various locations nevertheless arrive within a short succession of each other at a postsynaptic target.³⁹ The effect of myelination on signal transduction is quite profound with even slight changes in its thickness possessing the ability to bring about significant differences in the number of signals received by a specific neuron within a given time interval.^{39,40} This, in turn, might strongly affect local and global synchrony among neural groups. Therefore, it might be beneficial for the brain to dispose of the ability to dynamically adjust signal conduction among remote areas depending on the frequency with which they interact (engage in functional connectivity). Indeed, abundant biological evidence supports the idea of continued adaptive changes in myelination throughout the whole lifespan.^{33,34,36,41–43} The fact that adaptive myelination constitutes a second dynamic factor in addition to synaptic plasticity, both of which depend on the temporal statistics of neural activations in pre- and postsynaptic neuronal populations,³⁹ inspired us to systematically investigate their interactions in a system of weakly coupled oscillators. We employ a neural mass model to capture the phase evolution of weakly coupled neural groups as their connections undergo activity-dependent changes in coupling strength and conduction velocity.

Specifically, we consider a system of Kuramoto oscillators⁴⁴ with distance-dependent delays previously established to study the effect of synaptic plasticity.²³ We extend this model by dynamically adjusting conduction velocity (and hence transmission delays) in addition to synaptic weights. Changes in both synaptic weight and conduction depend on a Hebbian learning rule,²⁶ which is based on the frequency of the coactivations among pairs of network oscillators. That is, both connection weights and conduction velocity are time-dependent parameters influencing each other and the dynamics of the network as a whole.

II. MATERIALS AND METHODS

A. Weakly coupled oscillator model

In line with previous work,²³ our network model consists of an ensemble of N phase oscillators arranged along a circle, i.e., a one-dimensional array with periodic boundary conditions. The network is fully connected with the exact coupling strengths between oscillators given by the real-valued directed connectivity matrix K . Local dynamics of each phase oscillator are governed by a Kuramoto model with transmission delays,

$$\begin{cases} \dot{\varphi}_i(t) = \omega_i + \frac{1}{N} \sum_{j=1}^N K_{ij}(t) \sin(\varphi_j(t - \tau_{ij}) - \varphi_i(t)), & \tau_{ij} = \frac{d_{ij}}{v}, \\ \dot{\varphi}_i(t) = \omega_i + \frac{1}{N} \sum_{j=1}^N K_{ij}(t) \sin(\varphi_j(t - \tau_{ij}(t)) - \varphi_i(t)), & \tau_{ij}(t) = \frac{d_{ij}}{v_{ij}(t)}, \end{cases} \quad (1)$$

where $\varphi_i(t) \in [0, 2\pi)$ denotes the phase of oscillator i ($i = 1, \dots, N$) at time t , ω_i is its intrinsic frequency, and K_{ij} reflects the strength of the connection from the j th to the i th oscillator. The transmission delay from j to i is static (τ_{ij}) if conduction velocity is constant (v),

or time-dependent ($\tau_{ij}(t)$) if conduction velocity is dynamic [$v_{ij}(t)$, see Eq. (4)]. Finally, d_{ij} is the distance between two oscillators. Due to periodic boundary conditions, this distance can be defined as

$$d_{ij} = \frac{L}{N} \min(|i - j|, N - |i - j|), \quad (2)$$

with L controlling the circumference of the circle. For the case of static delays, we define a coupling delay constant $T = \frac{L}{v}$ as the time needed for signals traveling at a velocity v to revolve once around the circle.²³

The coupling strength K_{ij} between oscillators i and j varies dynamically according to a form of Hebbian learning where the growth or decay of coupling strengths depend on the phase offset between oscillators,^{45,46}

$$\begin{cases} \dot{K}_{ij}(t) = \varepsilon_s [\alpha_s \cos(\varphi_i(t) - \varphi_j(t - \tau_{ij})) - K_{ij}(t)], & \tau_{ij} = \frac{d_{ij}}{v}, \\ \dot{K}_{ij}(t) = \varepsilon_s [\alpha_s \cos(\varphi_i(t) - \varphi_j(t - \tau_{ij}(t))) - K_{ij}(t)], & \tau_{ij}(t) = \frac{d_{ij}}{v_{ij}(t)}. \end{cases} \quad (3)$$

In Eq. (3), ε_s and α_s control the learning rate and learning enhancement factor of the coupling strength, respectively. The learning enhancement factor α_s determines the maximum and minimum coupling strength²² and ensures that these remain sufficiently weak.

For the case in which conduction velocities between pairs of oscillators vary dynamically, conduction velocity is no longer identical for all pairs of oscillators but varies according to a second Hebbian learning process,

$$\dot{v}_{ij}(t) = \varepsilon_v [\alpha_v \cos(\varphi_i(t) - \varphi_j(t - \tau_{ij}(t))) - v_{ij}(t)]. \quad (4)$$

Here, ε_v and α_v are the learning rate and learning enhancement factor of the conduction velocity, respectively. Note that conduction velocity was bounded from below because $v_{ij}(t)$ may otherwise grow too small leading to delays approaching infinity. We chose to bound $v_{ij}(t)$ at a value of 0.1 as this corresponds to $T = 10$ in the static case if all pairwise conduction velocities decay to this value.

B. Quantitative analyses

1. Global synchronization behavior

In a network of globally coupled oscillators arranged along a ring with distance-dependent delays, the distribution of phases may show propagating structures, static phase increments from one oscillator to the next, referred to as coherent-wave modes.^{23,47} Phase offsets with respect to a reference oscillator (e.g., the first) may exhibit periodicity at integer (or half-integer, see below) multiples of 2π . Frequency synchronization, identical frequencies but distributed phases, in such a system can thus be characterized in terms of these multiples of 2π , which are referred to as coherent-wave modes (denoted by m). However, for the system employed here, identification of coherent-wave mode values is complicated by the fact that either a single or two clusters of synchronized oscillators may form. We refer to the formation of a single cluster as single-cluster synchronization and to the formation of two (anti-phase) clusters as double-cluster synchronization. To overcome this problem, we measure both in-phase synchronization (r_1) and anti-phase synchronization

(r_2). In-phase synchronization is characterized by the generalized order parameter (r_1),^{44,48}

$$r_1 e^{i\psi(t)} = \frac{1}{N} \sum_{j=1}^N e^{i\varphi_j^*(t)}, \quad (5)$$

where $\psi(t)$ is the mean phase at time t ⁴⁴ and φ_j^* is the phase of oscillator j corrected for phase increments around the ring determined by the value of the mode m ⁴⁹

$$\varphi_j^*(t) = \varphi_j(t) \pm 2\pi m(j-1)/N. \quad (6)$$

Anti-phase synchronization is given by^{22,23}

$$r_2 = |r' - r_1|,$$

where

$$r' e^{i\psi'(t)} = \frac{1}{N} \sum_{j=1}^N e^{2i\varphi_j^*(t)}. \quad (7)$$

The term r' measures the in-phase and anti-phase synchronization by stretching the range from zero to π around the full circle. Hence, this measure needs to be adjusted for in-phase synchronization to obtain a measure of anti-phase synchronization (r_2). In accordance with previous work,²³ we used a threshold on r_2 to determine the presence of a second cluster (here $r_2 \geq 0.15$). This implies that a second (smaller) cluster may exist even though $r_1 > r_2$.

To determine the mode of the system and whether it exhibits single- or double-cluster synchronization in any particular simulation, we compute both r_1 and r_2 for a range of candidate mode values ($m \in \{0, 0.5, 1, 1.5, 2\}$) and select the mode that maximizes the global phase-coherence [$\max(r_1, r_2)$]. Please note that for double-cluster synchronization, m may take on half-integer values.²³ This procedure, while able to detect double-clustered states when clusters are of unequal size, can only do so if the phase offset between clusters equals π . This does not imply that two clusters may not exhibit smaller phase offsets.

2. Pairwise connectivity

In addition to the global synchronization behavior of the system, we also examine its local (i.e., pairwise) structural and functional connectivity. Structural connectivity is straightforwardly given by the coupling strength matrix K ranging from $-\alpha_s$ to α_s . To measure functional connectivity, we introduce a coherence matrix D whose elements are given by

$$D_{ij} = \frac{1}{\Delta t} \int_{t_r}^{t_r + \Delta t} \cos(\varphi_i(t) - \varphi_j(t)) dt. \quad (8)$$

Here, t_r marks a time-point after which the system no longer experiences major changes in coupling strength and/or conduction velocity. D_{ij} ranges from -1 to 1 with a value of 1 indicating that two nodes are in phase (over a time interval Δt) whereas a value of -1 indicates that two nodes are in anti-phase.

3. Numerical simulations

We analyze the system in terms of its global synchronization behavior as well as in terms of pairwise structural and functional

TABLE I. Network parameters.

Network parameter	Value
N	100
L	1

connectivity for three different cases: (I) dynamic coupling strength and static conduction velocity (cf. Ref. ²³); (II) static coupling strength and dynamic conduction velocity; and (III) dynamic coupling strength and dynamic conduction velocity. For the first scenario, the system is evaluated for a range of combinations of parameters ε_s and T . For the latter two scenarios, ε_s is fixed at either 0 (no learning, scenario II) or 0.1 (fast learning, scenario III), and the behavior is observed while the parameters ε_v and α_v are varied. The long-term behavior of the system is characterized by its coherent-wave mode of synchronization and its cluster-formation. For notational convenience, we denote each final state $\{m, c\}$, where m indicates the (half-)integer value of the coherent-wave mode and c indicates whether the network exhibits single (s) or double (d) cluster synchronization. For example, the state $\{1, d\}$ describes a system exhibiting double-cluster synchronization and a mode of 1.

For all simulations, intrinsic frequencies ω_i are drawn from a normal distribution $\mathcal{N}(1, 0.01)$ and initial phases are drawn from a uniform distribution in the range $[0, 2\pi)$. All simulations start from a network with coupling strengths fixed at their maximum value ($\alpha_s = 1$), which exceeds the critical coupling strength and supports interactions among oscillators. Furthermore, for those simulations for which velocity changes dynamically, conduction velocities are initialized as $v_{ij}(t=0) = 0.14$, which means that initial coupling delays correspond to the scenario where the delay constant (T) is ~ 7 for a ring length of $L = 1$. Parameters characterizing the network are summarized in Table I, while those characterizing the three simulated scenarios are summarized in Table II.

The model is implemented in MATLAB (R2016a) and integrated for 20 000 time steps using the forward Euler method with a step size $dt = 0.01$ in arbitrary units of time. To accommodate for delays, we always first simulate 1000 time steps during which oscillators are noninteracting. Subsequently, the time delay interaction is switched on to simulate the 19 000 time steps of interest.

TABLE II. Simulation parameters.

Scenario	Parameter	Value
Dynamic coupling strengths, static conduction velocities	α_s	1
	ε_v	0
	α_v	0
Static coupling strengths, dynamic conduction velocities	ε_s	0
	α_s	1
Dynamic coupling strengths and conduction velocities	ε_s	0.1
	α_s	1

We perform 50 simulations with different randomizations of initial conditions for each parameter combination in every scenario. We select the most frequently observed combination of coherent-wave mode of synchronization and cluster-formation (single vs double) as the characteristic final state of a given parameter combination. Whenever the characteristic state is observed in less than 70% of the simulations, we additionally identify a secondary state as the one occurring for at least 50% of the remaining simulations (i.e., of those not classified as the characteristic state). In this case, we regard the system as bistable. If no secondary state can be unambiguously identified and individual simulations yield different states, we regard the system as multistable. This procedure assumes that states are discernible for individual simulations; that is, they are indeed characterizable in terms of a unique combination of coherent-wave

mode of synchronization and cluster-formation. This assumption may be violated if the system remains incoherent or by the formation of chimera-like states, i.e., different subsets of oscillators exhibit distinct dynamical behaviors.^{50–54} In this case, we regard the system as erratic.

III. RESULTS

A. Scenario I: Dynamic coupling strengths, static conduction velocities

We first examined learning in the context of static conduction velocity. For this purpose, we explored a parameter space defined by the delay constant T and the learning rate ε_s . Most parameter settings

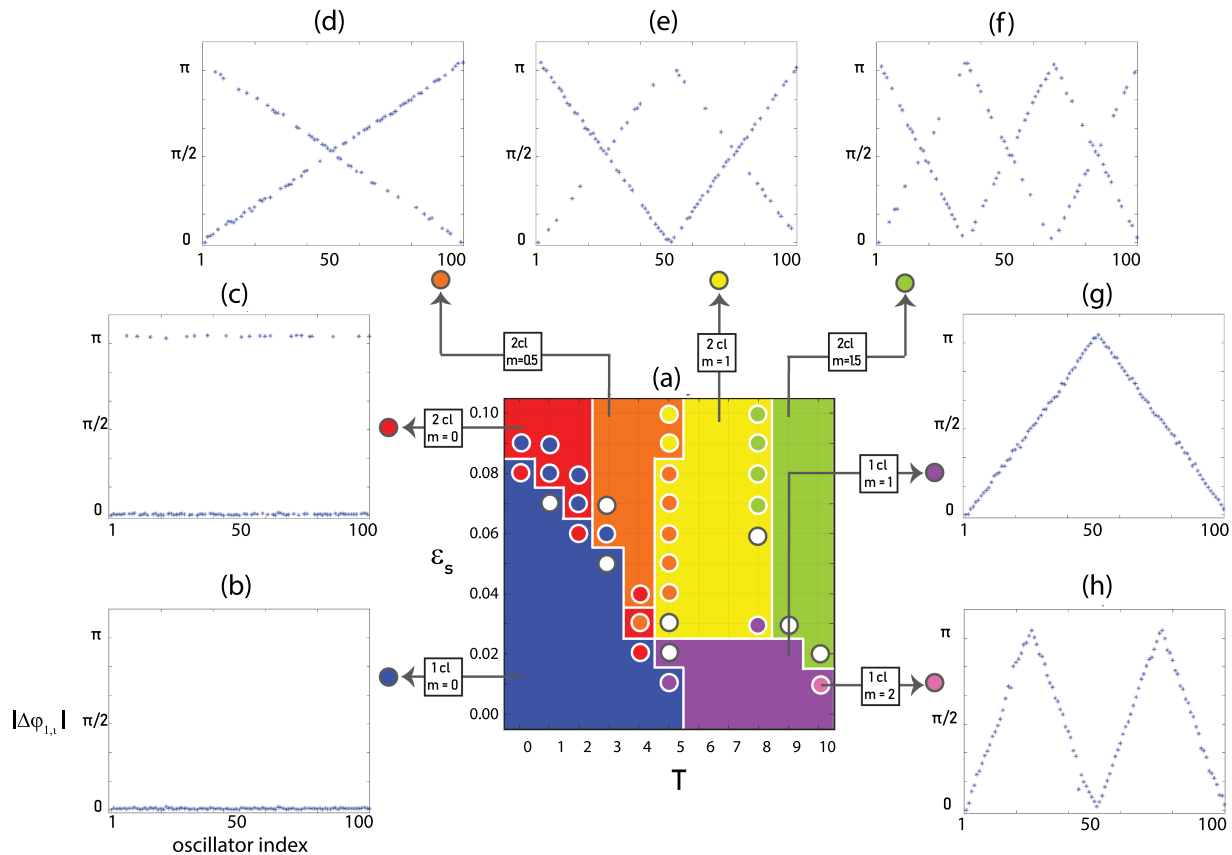


FIG. 1. Arrangement of phase offsets with respect to the first oscillator when the coupling strength is dynamic and the conduction velocity is static. Panel (a) shows the color-coded state (coherent-wave mode of synchronization and cluster-formation) for each point in the parameter space defined by T and ε_s . Colors indicate the characteristic states. Furthermore, colored disks indicate secondary states (bistability). A white disk indicates multistability. Panel (b) shows absolute phase offsets between every oscillator and the first ($|\Delta\varphi_{1,i}|$) for the state $\{0,s\}$. All offsets are close to zero. Panel (c) shows $|\Delta\varphi_{1,i}|$ for the state $\{0,d\}$. Phase offsets are close to zero for oscillators falling into the same cluster as the first and close to π (half period) for those falling into the opposite cluster. Panel (d) shows $|\Delta\varphi_{1,i}|$ for the state $\{0.5,d\}$. Phase offsets exhibit one half-cycle, i.e., oscillators falling into the same cluster as the first increases with distance, whereas those in the opposite cluster decrease with distance. Panel (e) shows $|\Delta\varphi_{1,i}|$ for the state $\{1,d\}$. Phase offsets exhibit one full cycle with offsets for oscillators falling into the same cluster as the first mirroring those of oscillators in the opposite cluster. Panel (f) shows $|\Delta\varphi_{1,i}|$ for the state $\{1.5,d\}$. Phase offsets exhibit one and a half cycles with offsets for oscillators falling into the same cluster as the first mirroring those of oscillators in the opposite cluster. Panel (g) shows $|\Delta\varphi_{1,i}|$ for the state $\{1,s\}$. Phase offsets exhibit one full cycle. Panel (h) shows $|\Delta\varphi_{1,i}|$ for the state $\{2,s\}$. Phase offsets exhibit two full cycles passed by a single cluster. All phase offsets are averaged over the last 100 time steps. Phase offsets for each parameter combination are shown in Fig. S1(b) in the [supplementary material](#).

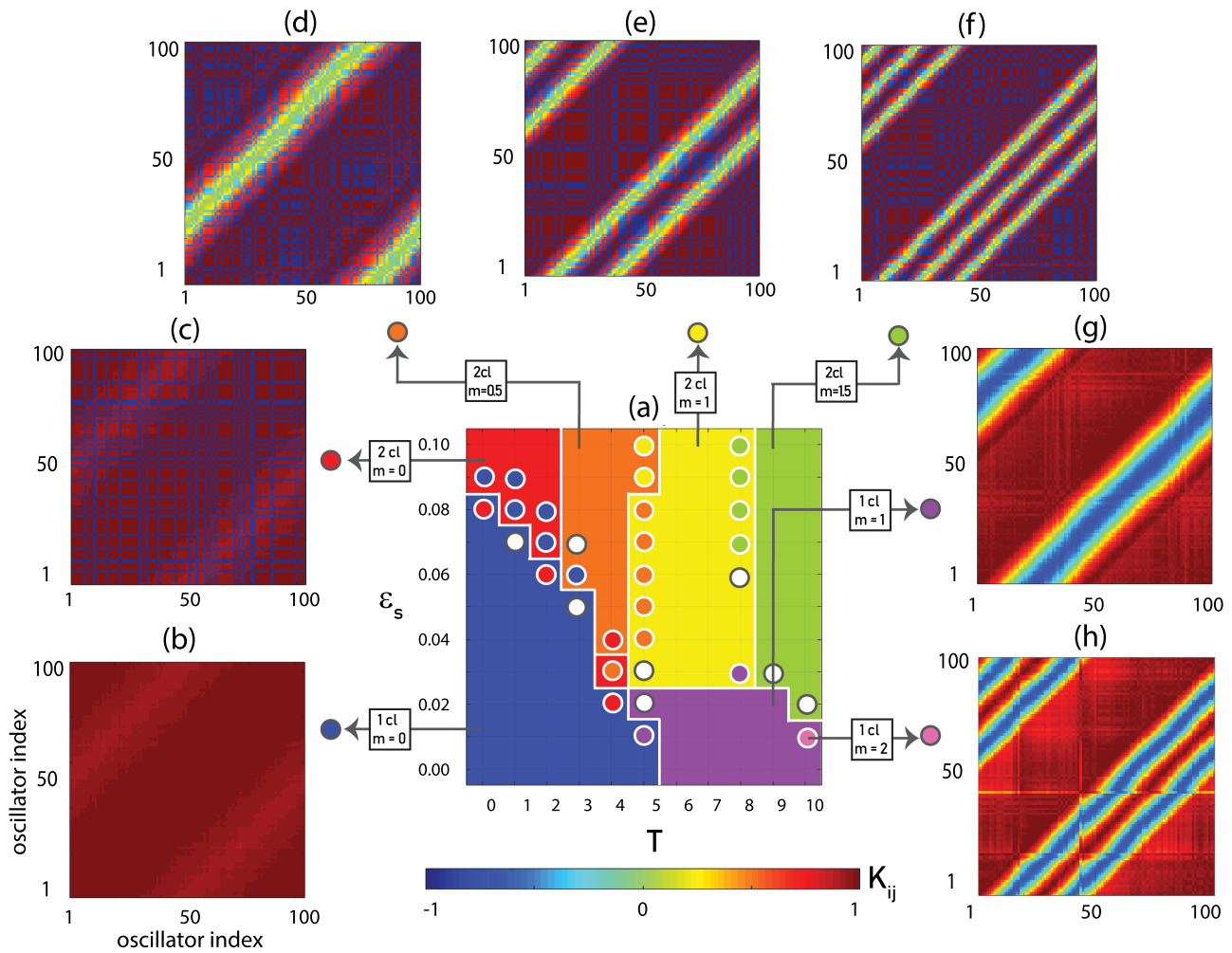


FIG. 2. Pairwise structural connectivity emerging in the context of dynamic coupling and static conduction. Panel (a) shows the color-coded state of coherent-wave mode of synchronization and cluster-formation observed at each point in the parameter space defined by T and ϵ_s . As in Fig. 1, the secondary state (bistability) is marked with colored disks, whereas white indicates multistability. Panel (b) shows the structural connectivity matrix of the network for the state $\{0,s\}$. The network largely preserves the initial connectivity pattern. Panel (c) shows structural connectivity of the network for the state $\{0,d\}$. Pairwise connection weights are close to $+\alpha_s$ and $-\alpha_s$ for oscillator pairs belonging to the same or distinct clusters, respectively. Panels (d)–(f) show structural connectivity matrices of the network for the state $\{0.5,d\}$ (d), state $\{1,d\}$ (e), state $\{1.5,d\}$ (f). As before, coupling weights have approached $+\alpha_s$ for within cluster connections and $-\alpha_s$ for between cluster connections. However, based on the mode synchronization, 1, 2, and 3 stripes of near-zero connection weights have formed in panels (d), (e), and (f), respectively. Panel (g) shows the structural connectivity matrix of the network for the state $\{1,s\}$. All possible phase offsets $((n - 1)(2\pi/N))$ with respect to the first oscillator can be observed. Panel (h) shows the structural connectivity matrix for a network given the state $\{2,s\}$. The same observations as for panel (g) can be made, with the difference that phase differences are repeated. The structural connectivity matrices are averaged over the last 100 time steps of the simulation. Structural connectivity matrices for each parameter combination are shown in Fig. S1(c) in the [supplementary material](#).

yield highly consistent results. However, some regions of parameter space exhibit diverse results. This is especially prevalent at borders between adjacent regions and likely reflects transitions in mode synchronization, cluster-formation, or both. At borders, the system may be multistable and the state observed for any given simulation depends on initial conditions. The two parameters affect the behavior of the system in different, albeit interacting, ways. The learning rate mainly affects cluster-formation, with slow learning leading to

the emergence of a single cluster while fast learning leads to the formation of two clusters [see Fig. 1(a)]. In the former case, changes in coupling strength between pairs of oscillators occur at a slower rate than synchronization. That is, the system synchronizes before large initial phase offsets can decrease coupling. In the latter case, changes in coupling strength between pairs of oscillators occur at a faster rate than synchronization. That is, initially large phase offsets between pairs of oscillators quickly drive their coupling strength to

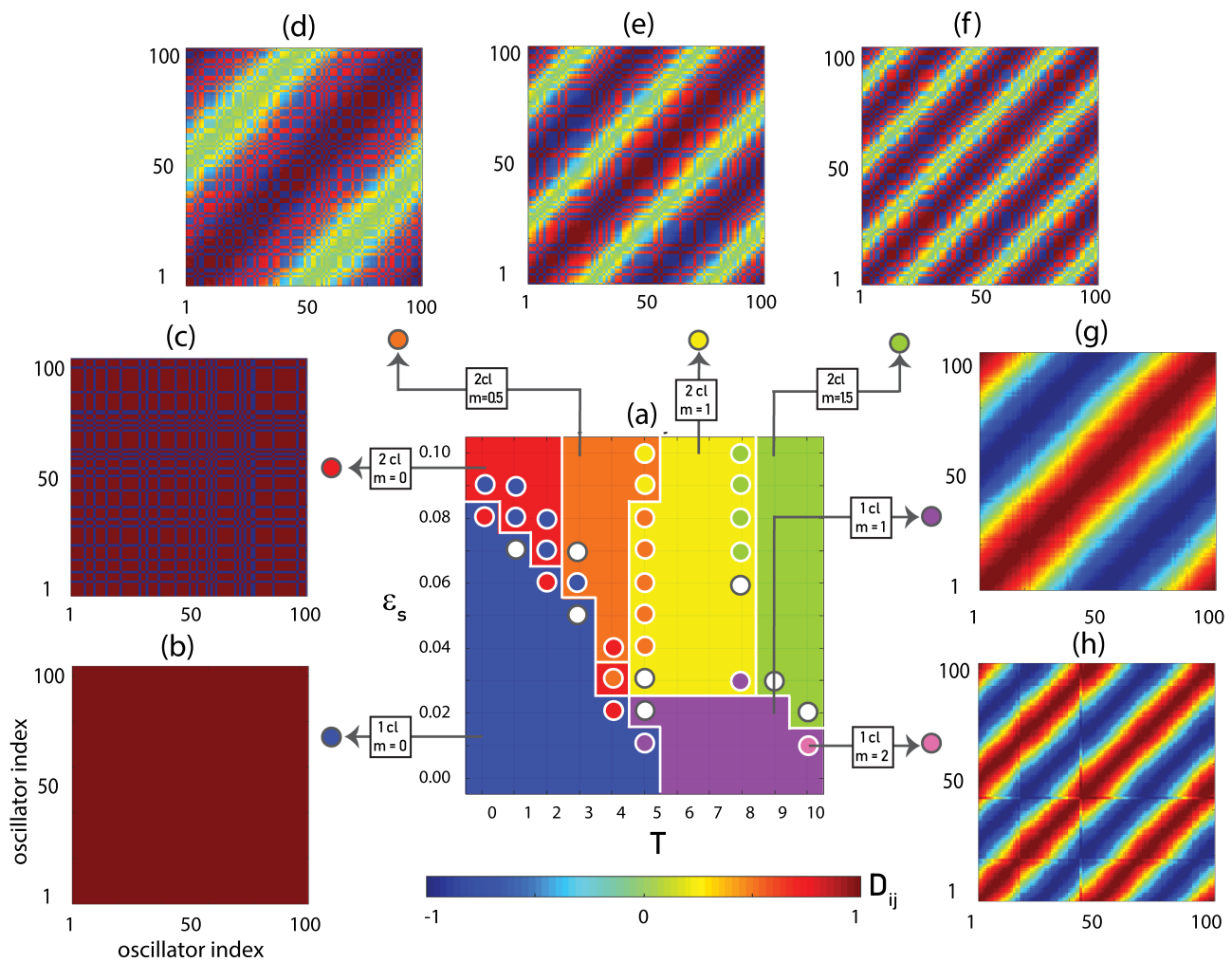


FIG. 3. Pairwise functional connectivity among oscillators emerging when the coupling strength is dynamic and the conduction is static. Panel (a) shows the color-coded state of coherent-wave mode of synchronization and cluster-formation observed at each point in the parameter space defined by T and ϵ_s . Color coding is the same as in Fig. 1. Panel (b) shows the functional connectivity matrix of the network for the state $\{0,s\}$. The globally correlated functional connectivity matrix resembles the structural connectivity matrix. Panel (c) shows the functional connectivity matrix of a network for the state $\{0,d\}$. Panels (d)–(f) show functional connectivity matrices of networks for the state $\{1.5,d\}$ (d), state $\{1,d\}$ (e), state $\{1.5,d\}$ (f). The functional pairwise correlations are associated with the cluster-formation of oscillators as they are 1 or close to 1 for intracluster correlations and are -1 or close to -1 for between cluster correlations. Based on the mode of synchronization, 2, 4, and 6 stripes of zero or very weak correlations in panels (d), (e), and (f) are formed, respectively. Panel (g) shows the functional connectivity matrix of a network for the state $\{1,s\}$. Pairwise functional connectivity values are 1 for the neighboring oscillators and decrease to -1 as a function of distance. Panel (h) shows the functional connectivity matrix of the network for the state $\{2,s\}$. A similar pattern as for panel (g) manifests, but reflecting two complete revolutions of phase offsets around the circle. The elements of correlation matrices were computed over the last 100 time steps of the simulation. Functional connectivity matrices for each parameter combination are shown in Fig. S1(d) in the [supplementary material](#).

negative values, thus exacerbating their offset until they are separated by exactly π .

The delay constant interacts with the learning rate as increasing delays allow for the formation of two clusters at progressively lower learning rates.⁵⁵ However, it mainly affects mode synchronization with longer delays leading to larger m (see Fig. 1). Specifically, for nonzero values, phases distribute around the circle such that the offset between each pair of neighboring oscillators is $\frac{2\pi}{N} m$ (within a cluster) or $\frac{2\pi}{N} m + \pi$ (across clusters). Note that for the emergence

of two clusters, half-integer values can be obtained [Figs. 1(d) and 1(f)]. This is in line with previous observations²³ that half-integer values are the result of the two clusters interconnecting. Oscillator pairs within a cluster “see” each other in phase when their phase offsets are matched by their delays. That is, due to delays, from the perspective of each oscillator in a cluster, the other oscillators within the same cluster appear in-phase, whereas to an external observer, they may appear out of phase. For the emergence of a single cluster, there is an exception to this observation for oscillator

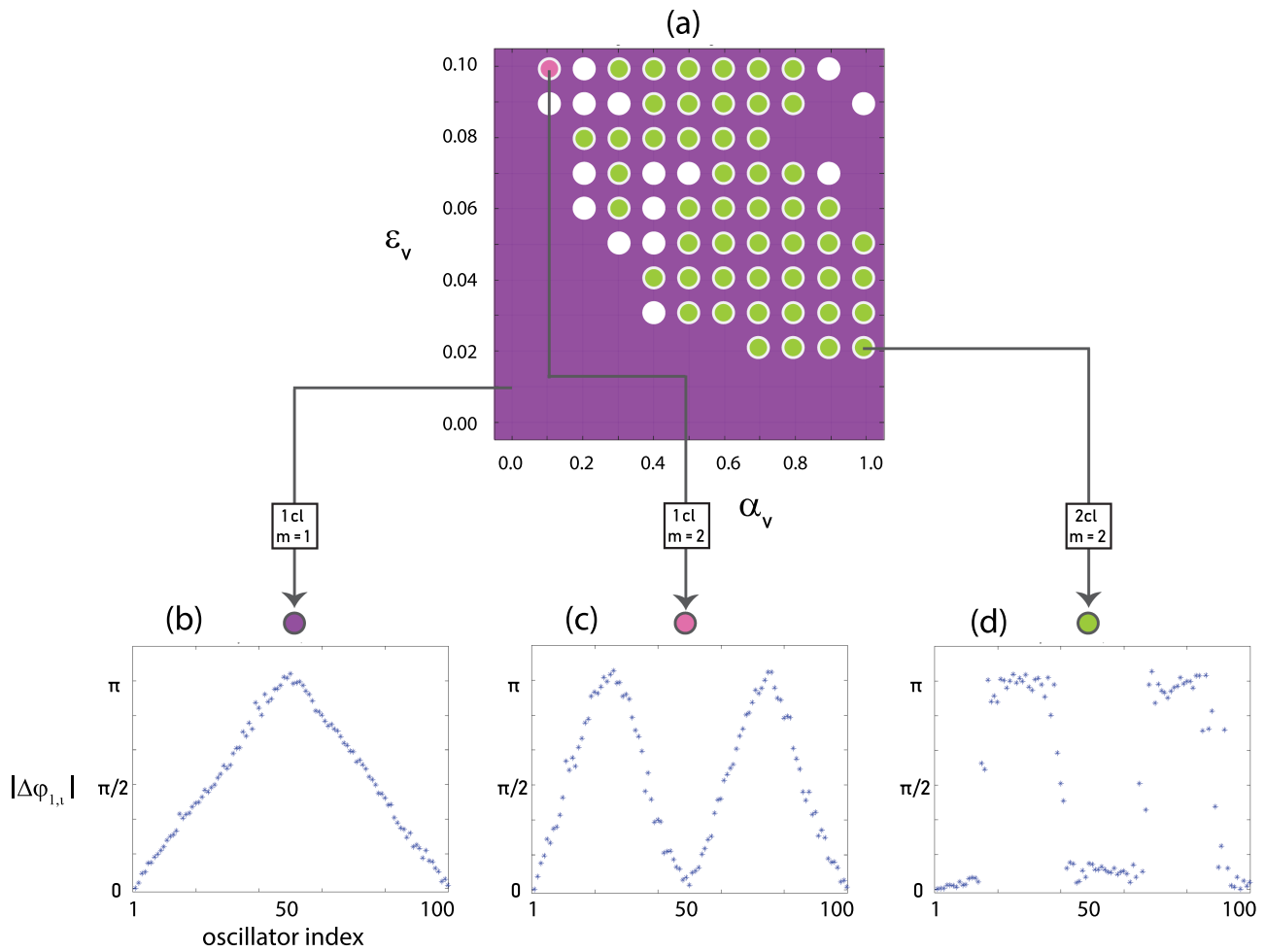


FIG. 4. Phase offsets with respect to the first oscillator when the coupling strength is static and the conduction is dynamic. Panel (a) shows the color-coded state of coherent-wave mode of synchronization and cluster-formation observed at each point in the parameter space defined by ε_v and α_v . Color coding is the same as in Fig. 1. The entire parameter space is primarily characterized by the state $\{1,s\}$. However, a wide region of parameter space exhibits a secondary state defined by a mode of 2 and the formation of two clusters. Panel (b) shows $|\Delta\varphi_{1,i}|$ for the state $\{1,s\}$. Phase offsets exhibit one full cycle. Panel (c) shows $|\Delta\varphi_{1,i}|$ for the state $\{2,s\}$. Phase offsets exhibit two full cycles. Panel (d) shows $|\Delta\varphi_{1,i}|$ for the state $\{2,d\}$. Phase offsets are largely pushed to either 0 or π , depending on the cluster affiliation. All phase offsets are averaged over the last 100 time steps. Phase offsets for each parameter combination are shown in Fig. S2(b) in the [supplementary material](#).

pairs with a phase offset around $\frac{\pi}{2}$. For these values, the trailing oscillator sees the leading oscillator in phase. However, the leading oscillator sees the trailing one in anti-phase. This asymmetry affects the coupling strength such that the structural connection from the leading to the trailing oscillator is positive while that from the trailing to the leading is negative. The magnitude of their coupling strength is otherwise equal. This leads to one or two stripes of negative values in the structural connectivity matrix for modes $m = 1$ and $m = 2$, respectively [see Figs. 2(g) and 2(h)]. Interestingly, the structural connectivity matrices emerging for double-cluster-formation also exhibit stripes for nonzero modes [Figs. 2(d)–2(f)]. The number of these stripes in each case is twice its corresponding mode value m . According to the Hebbian learning rule [Eq. (4)], coupling strengths between every two oscillators i and j approach a

stable value given by $K_{ij} = \alpha_s \cos(\varphi_i - \varphi_j)$. For phase differences of $(2n - 1)\frac{\pi}{2}$, this entails that the connection weights between the corresponding oscillators decay to zero. Since the mode determines the repetition of phase offsets equal to $(2n - 1)\frac{\pi}{2}$ for each oscillator, it also determines the number of stripes in the structural connectivity matrices.

The emergence of stripes is also apparent in functional connectivity matrices (Fig. 3). Here, stripes are symmetric, however, since functional connectivity is undirected. Therefore, twice as many stripes can be observed in functional connectivity matrices as compared to structural connectivity matrices. Furthermore, the exact location of stripes in the structural and functional connectivity matrices is different because temporal delays are not considered in the computation of pairwise correlations.

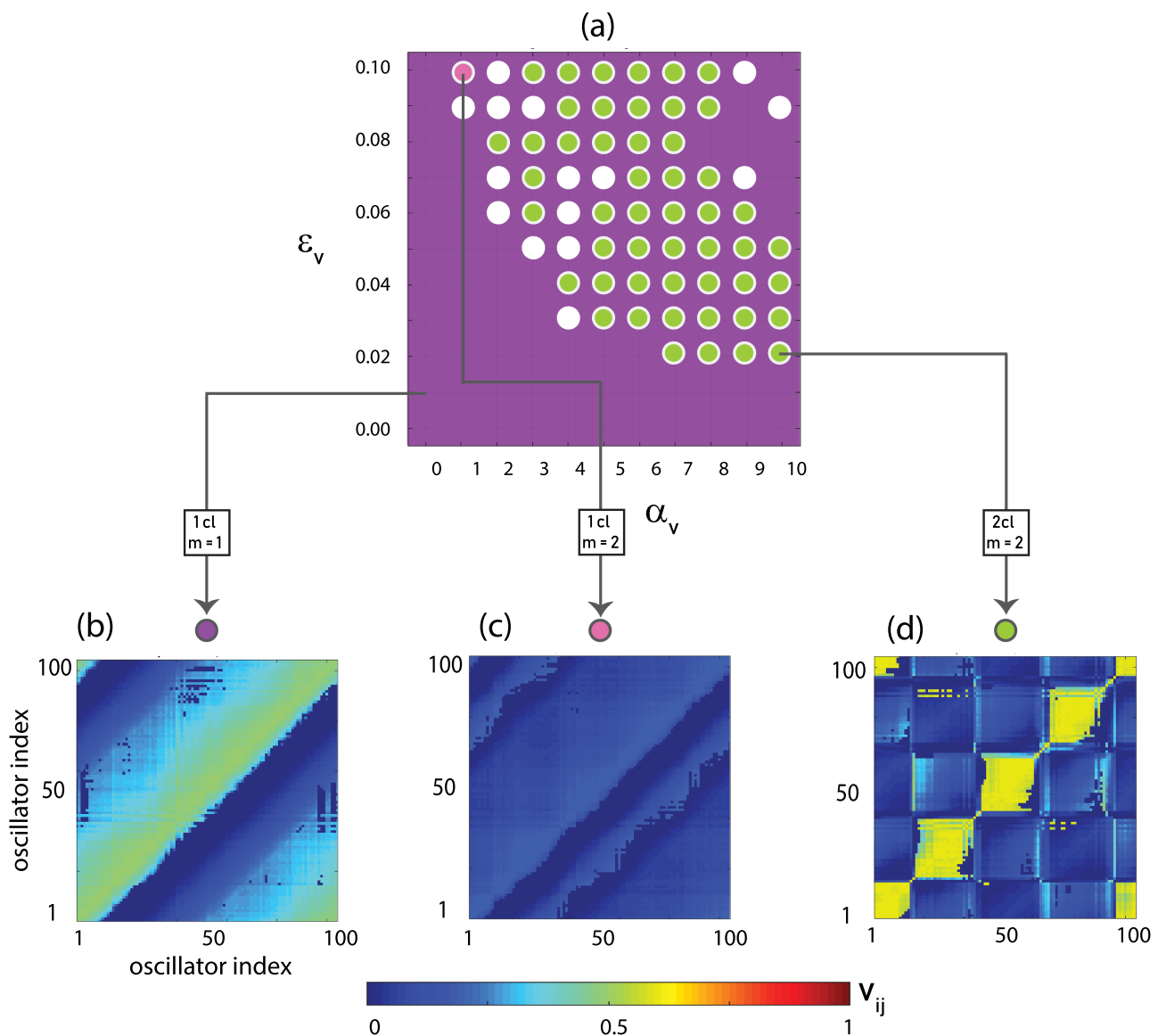


FIG. 5. Conduction velocity matrices when the coupling strength is static and the conduction is dynamic. Panel (a) shows the color-coded state of coherent-wave mode of synchronization and cluster-formation observed at each point in the parameter space defined by ϵ_v and α_v . Color coding is the same as in Fig. 1. Panels (b) and (c) show the pairwise conduction velocity matrices for the state $\{1,s\}$ (reflecting one full cycle of phase offsets) and the state $\{2,s\}$ (reflecting two full cycles of phase offsets), respectively. Panel (d) shows the pairwise conduction velocity matrices for the state $\{2,d\}$. Conduction velocities between the intracluster oscillators are noticeably higher than those between other pairs. The conduction velocity matrices are averaged over the last 100 time steps of the simulation. Conduction velocity matrices for each parameter combination are shown in Fig. S2(c) in the [supplementary material](#).

B. Scenario II: Static coupling strengths, dynamic conduction velocities

Next, we examine the effects of dynamic conduction velocity on a network with static connection weights to establish the unique effects of adaptive myelination on functional connectivity among phase oscillators. To that end, we vary the learning rate ϵ_v and

enhancement factor α_v controlling dynamic changes in conduction velocity. Note that we no longer vary the coupling delay constant T since delays depend on conduction. Rather, we initialize conduction velocity among oscillator pairs such that $v_{ij}(t = 0) = 0.14$, which means that the initial coupling delays correspond to the case where $T \cong 7$. These parameter settings correspond to a system exhibiting state $\{1,s\}$ in simulations where conduction remains static.

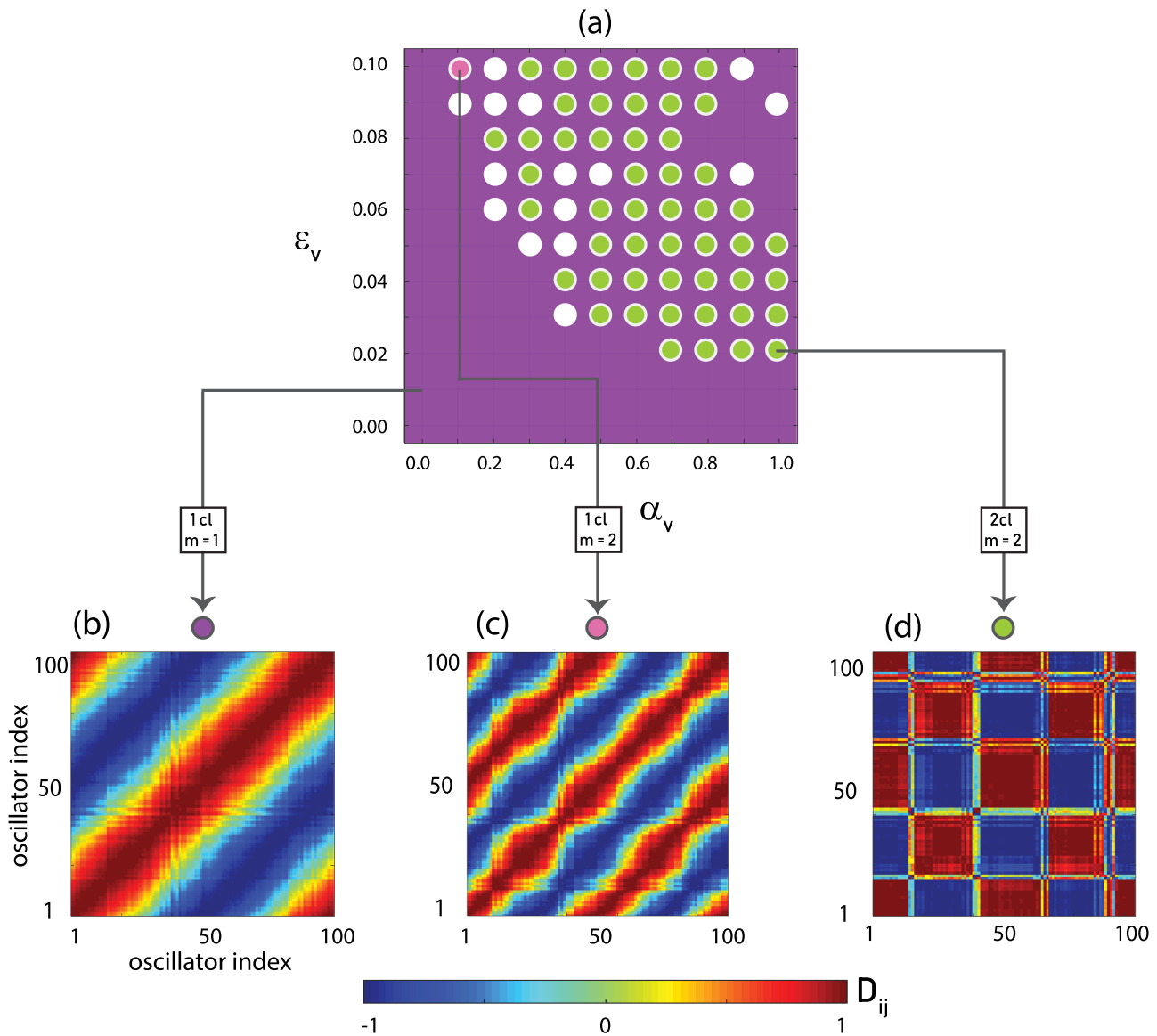


FIG. 6. Pairwise functional connectivity among oscillators when the coupling strength is static and the conduction is dynamic. Panel (a) shows the color-coded state of coherent-wave mode of synchronization and cluster-formation observed at each point in the parameter space defined by ϵ_v and α_v . Color coding is the same as in Fig. 1. Panel (b) shows a representative functional connectivity matrix of the network for the state $\{1,s\}$. The matrix reflects a full cycle of phase offsets. Panel (c) shows a functional connectivity matrix of the network for the state $\{1,s\}$. Two complete revolutions of the relative phase offsets are exhibited. Panel (d) shows a functional connectivity matrix of the network for the state $\{2,d\}$. A vast majority of the pairwise correlations reflect either in-phase or anti-phase relations among oscillators. The correlation matrices were computed over the last 100 time steps of the simulation. Functional connectivity matrices for each parameter combination are shown in Fig. S2(d) in the [supplementary material](#).

For dynamic conduction velocity, state $\{1,s\}$ is still observed most frequently irrespective of the values chosen for ϵ_v and α_v . However, within a contiguous region of parameter space, the system exhibits state $\{2,d\}$ as its secondary state, which is indicative of bistability [Fig. 4(a)]. Furthermore, at the borders of this region, the system exhibits a highly variable behavior, indicative of multistability.

Figure 4 shows absolute phase offsets of all oscillators with respect to the first. Remarkably, for state $\{2,d\}$, phases cluster around 0 and π with sharp transitions between the two rather than smooth transitions. In fact, dynamic conduction velocity pushes phase offsets to either 0 or π , which brings about a transformation from state $\{2,s\}$ to state $\{2,d\}$. This localized clustering leads to highly structured

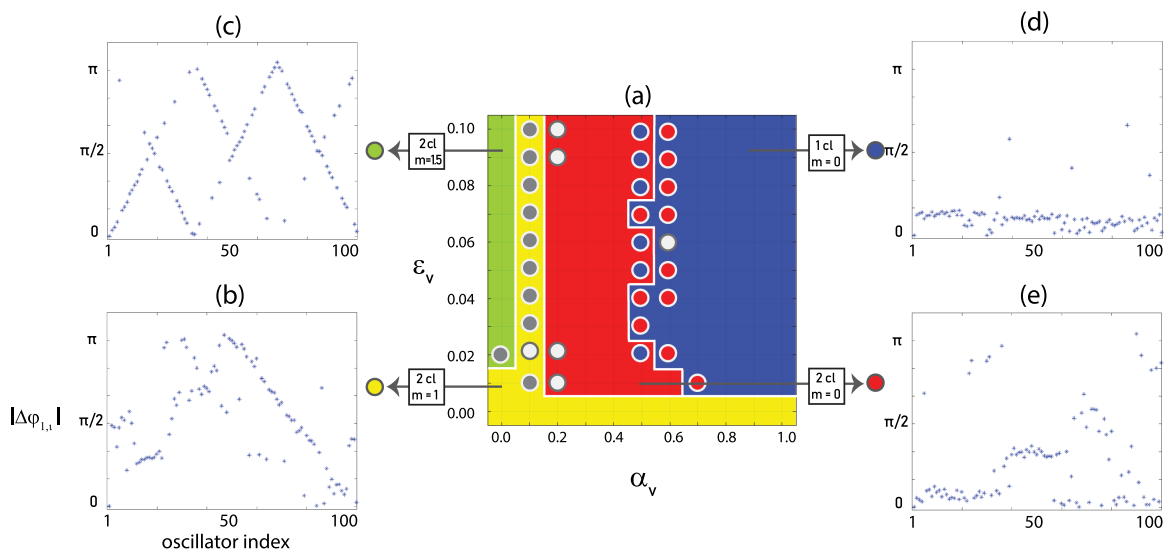


FIG. 7. Phase offsets with respect to the first oscillator when the coupling strength and the conduction velocity are both dynamic. Panel (a) shows the color-coded state of coherent-wave mode of synchronization and cluster-formation observed at each point in the parameter space defined by ϵ_v and α_v . Color coding is the same as in Fig. 1. Gray circles mark erratic states. Panel (b) shows $|\Delta\varphi_{1,i}|$ for the state $\{1,d\}$. Panel (c) shows $|\Delta\varphi_{1,i}|$ for the state $\{1.5,d\}$. Phase offsets exhibit one and a half cycles. Panel (d) shows $|\Delta\varphi_{1,i}|$ for the state $\{0,s\}$. Aside from a few exceptions, offsets are generally close to zero. Panel (e) shows $|\Delta\varphi_{1,i}|$ for the state $\{0,d\}$. While our procedure identified this example as 0-mode synchronization, visually it appears to not fit any state particularly well. Phase offsets were averaged over the last 100 time steps. Phase offsets for each parameter combination are shown in Fig. S3(b) in the [supplementary material](#).

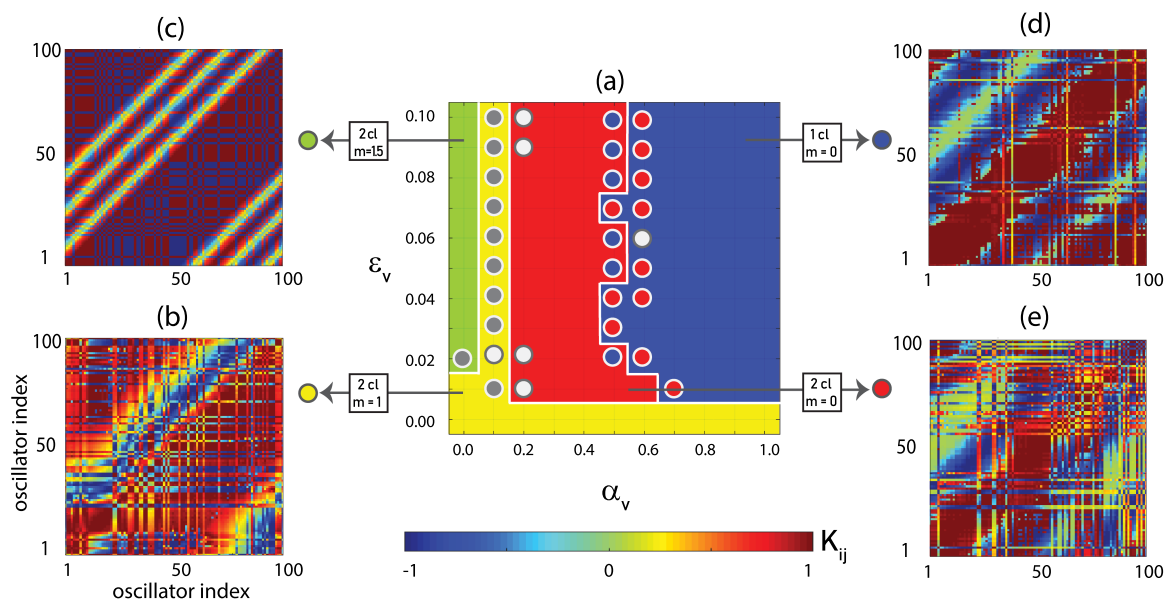


FIG. 8. Pairwise structural connectivity emerging when the coupling strength and the conduction velocity are both dynamic. Panel (a) shows the color-coded state of coherent-wave mode of synchronization and cluster-formation observed at each point in the parameter space defined by ϵ_v and α_v . Color coding is the same as in Fig. 1 (gray disks as in Fig. 7). Panel (b) shows structural connectivity of the network for the state $\{1,d\}$. Panel (c) shows structural connectivity matrix of the network for the state $\{1.5,d\}$. As for simulations with static conduction velocity, in this region, connectivity matrices exhibit 3 ($2m$) stripes reflecting weak connections. Panel (d) shows structural connectivity of the network for the state $\{0,s\}$. Panel (e) shows structural connectivity of the network for the state $\{0,d\}$. The structural connectivity matrices are averaged over the last 100 time steps of the simulation. Structural connectivity matrices for each parameter combination are shown in Fig. S3(c) in the [supplementary material](#).

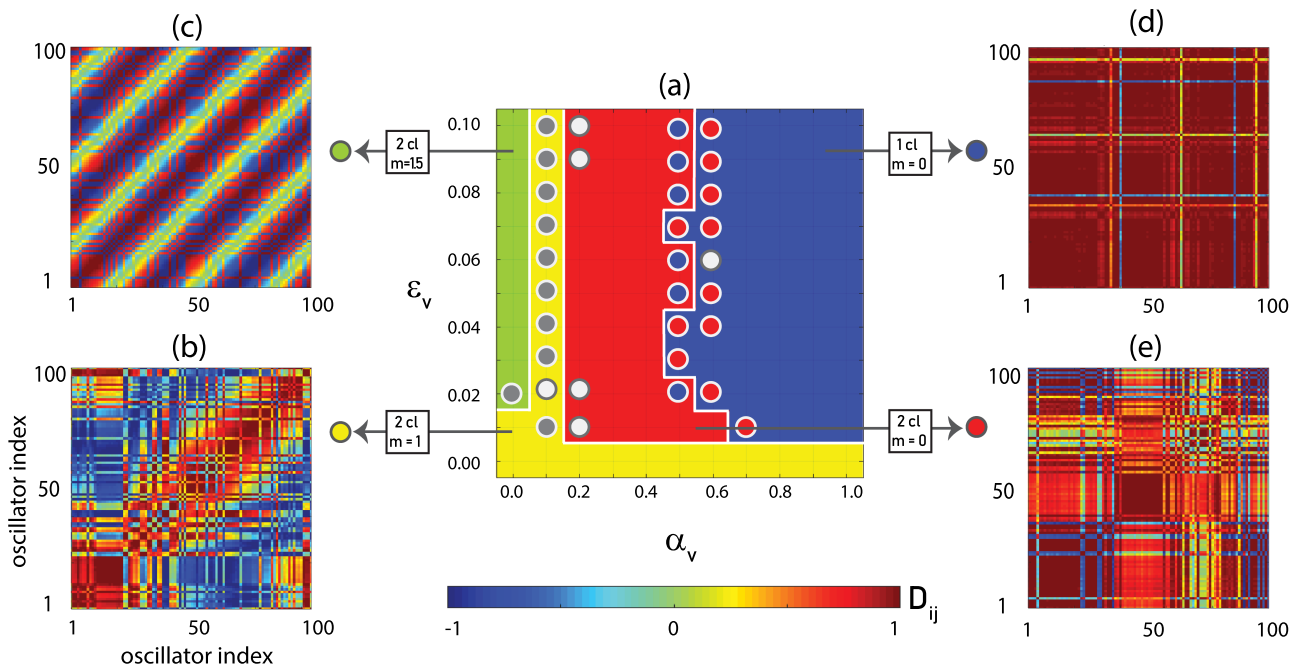


FIG. 9. Pairwise functional connectivity among oscillators when the coupling strength and the conduction velocity are both dynamic. Panel (a) shows the color-coded state of coherent-wave mode of synchronization and cluster-formation observed at each point in the parameter space defined by ϵ_v and α_v . Color coding is as in Fig. 1 (gray disks as in Fig. 7). Panel (b) shows functional connectivity of the network for the state $\{1,d\}$. Panel (c) shows functional connectivity of the network for the state $\{1.5,d\}$. The formation of $4m$ stripes of zero or very weak connection weights can be observed. Panel (d) shows the functional connectivity matrix for a network of the state $\{0,s\}$. Panel (e) shows the functional connectivity matrix for a network of the state $\{0,d\}$. Correlation matrix elements are averaged over the last 100 time steps of the simulation. Functional connectivity matrices for each parameter combination are shown in Fig. S3(e) in the supplementary material.

clusters, where an oscillator’s affiliation with a cluster is determined by its location along the ring rather than by randomly distributed initial phase values. Interestingly, conduction matrices emerging for state $\{2,d\}$ suggest that the system exhibits four distinct clusters rather than two [see Fig. 5(d)], one cluster for each peak and trough of the phase offsets [cf. Fig. 4(d)]. That is, signals are conducted fast among oscillators within a peak (trough) and slow among oscillators across peaks (troughs). This is the result of initial conditions. With conduction velocity being equal, short distances among oscillators within a peak (trough) lead to short delays, whereas long distances across peaks (troughs) lead to long delays. In this case, the pressure to synchronize peaks (troughs) is most easily met when signals are transmitted instantaneously within a peak (trough) or with a delay matching exactly one period across peaks (troughs). Functionally, these four clusters are not discernible [see Fig. 6(d)] since oscillators falling into both peaks (troughs) exhibit no phase offset with respect to each other.

C. Scenario III: Dynamic coupling strengths and conduction velocities

Having explored the effects of dynamic structural connectivity and dynamic conduction velocity in isolation, we next investigate their interaction. Dynamic changes in connection strength and conduction velocity constitute the most biologically relevant scenario.

In this simulation, initial values of the conduction velocity matrix v were again chosen such that they resemble the condition where $T \cong 7$. Furthermore, the learning rate ϵ_s was fixed at 0.1 (fast learning). Recall that this configuration produces state $\{1,d\}$ for static conduction velocity [cf. Fig. 1(a)]. As for scenario II, we explore the parameter space defined by the enhancement factor α_v and the learning rate ϵ_v controlling dynamic conduction velocity. Figure 7(a) reveals that the behavior of the system is mainly affected by the enhancement factor α_v , which determines the maximum conduction velocity. If the learning rate ϵ_v is small, conduction velocity changes too slowly to have any discernible influence on the behavior of the system and state $\{1,d\}$ is preserved for all values of α_v . Once the conduction learning rate ϵ_v is sufficiently large, however, the behavior of the system is entirely determined by α_v . Note that in this case, the rate of change in conduction velocity may be still a factor of 10 smaller than the learning rate controlling synaptic plasticity.

For values of $\alpha_v < 0.14$, conduction necessarily decays toward values lower than initialization. This produces a situation essentially equivalent to fast learning and very long delays ($T \geq 9$) in scenario I and leads to the emergence of state $\{1.5,d\}$ [cf. Fig. 1(f)]. For $\alpha_v \cong 0.14$, the system frequently exhibits erratic behavior. To account for the system’s behavior as α_v increases, it is essential to consider the fact that both coupling strengths and conduction velocities evolve according to the same Hebbian learning rule with the sole difference

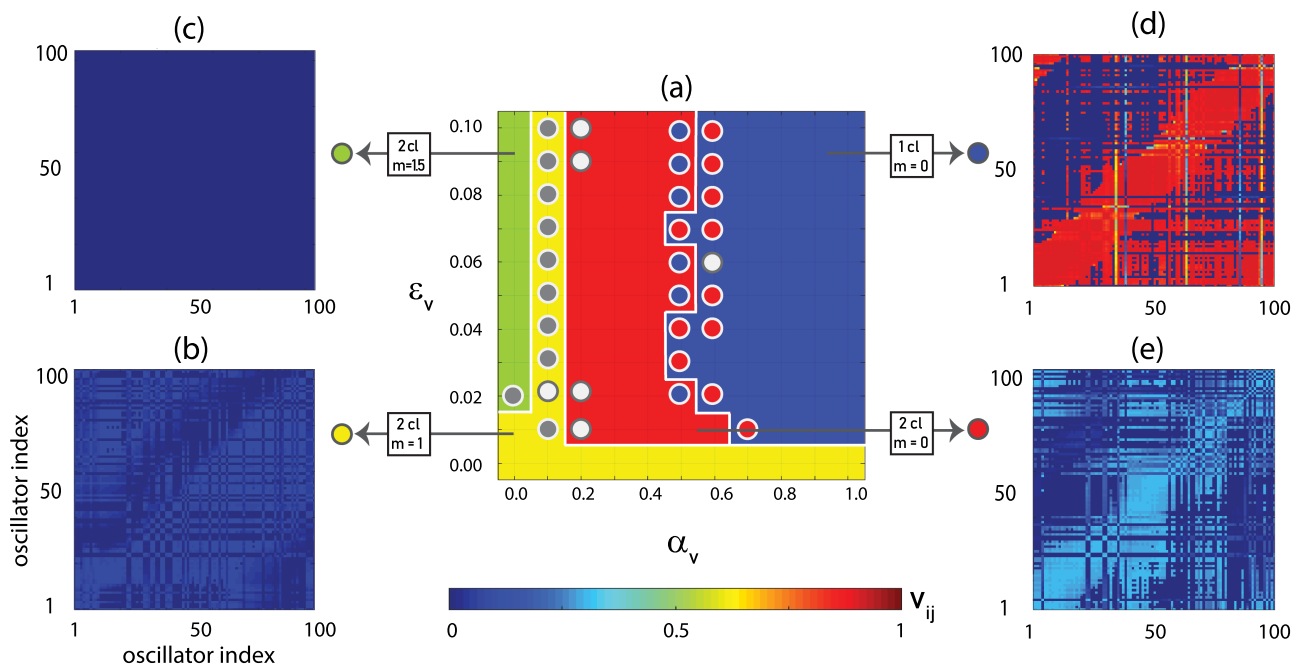


FIG. 10. Pairwise conduction velocities among oscillators when the coupling strength and the conduction velocity are both dynamic. Panel (a) shows the color-coded state of coherent-wave mode of synchronization and cluster-formation observed at each point in the parameter space defined by ϵ_v and α_v . Color coding is the same as in Fig. 1 (gray disks as in Fig. 7). Panel (b) shows the pairwise conduction velocity of the network for the state $\{1, d\}$. Conduction velocities only change slightly relative to their initial values. Panel (c) shows pairwise conduction velocity of the network for the state $\{1.5, d\}$. Conduction velocities have decayed to zero. Panel (d) shows pairwise conduction velocity of the network for the state $\{0, s\}$. Panel (e) shows pairwise conduction velocity of the network for the state $\{0, d\}$. The conduction velocity matrices are averaged over the last 100 time steps of the simulation. Conduction velocity matrices for each parameter combination are shown in Fig. S3(d) in the [supplementary material](#).

that conduction velocities are bounded from below at 0.1. This implies that whenever the coupling strength between two oscillators tends toward $+\alpha_s$, conduction velocity between the two increases (toward α_v). In contrast, whenever the coupling strength between two oscillators tends toward $-\alpha_s$, coupling velocity between the two decreases (toward 0.1). This implies that coupling strength and conduction velocity act agonistically for oscillators within the same cluster; these oscillators are both positively coupled and exhibit fast conduction velocity (short delays). However, for oscillators in separate clusters, coupling strength and conduction velocity act antagonistically. Negative coupling is paired with slow conduction velocity (long delays). For intermediate values of α_v , oscillators in different clusters see each other in anti-phase for phase offsets smaller than π . They thus form two clusters whose offset is less than half a period (depending on the exact offset, our procedure may label them as single or double cluster; see the boundary between red and blue regions in Fig. 7). For large values of α_v , oscillators in different clusters see each other in anti-phase for phase offsets close to zero [Fig. 7(d)]. This allows them to form a single functional cluster [Fig. 9(d)] even though they may be structurally segregated, both in terms of coupling strength [Fig. 8(d)] and conduction velocity [Fig. 10(d)]. The system can thus exhibit a wide array of states not observed when considering dynamic coupling strength alone.

IV. DISCUSSION

In the present study, we investigated the effects of dynamic coupling strength and dynamic conduction velocity on the synchronization behavior of weakly coupled oscillators arranged on a circle. For dynamic coupling strength combined with static conduction velocity, we found that, depending on the learning rate controlling changes in coupling strength, a single or two clusters can emerge. This is in line with previous studies on dynamic coupling in the Kuramoto model.²² Furthermore, depending on the delay, phase offsets may exhibit periodicity according to coherent-wave modes of synchronization.^{22,23} For nonzero modes, structural clusters become functionally apparent only after correcting for offsets. For zero modes, a tight correspondence between structural and functional clusters is straightforwardly apparent. This is no longer the case once conduction velocity is allowed to vary. Already in the context of static coupling strength, we observed that dynamic conduction velocity dissociates structural from functional connectivity. In terms of coupling strength, the system may appear as a single cluster. However, in terms of conduction velocity, which is another structural aspect, a wide range of parameters leads to the formation of four distinct clusters with fast communication within clusters and slow communication across clusters. Interestingly, communication between neighboring clusters is, while slower than within clusters, faster than between non-neighboring

clusters. This leads to the emergence of two functional clusters. Oscillator pairs with either very fast and very slow communication see each other in phase since phase offsets are either close to zero or some integer multiple of 2π and hence form a single functional cluster. This cluster is spatially discontinuous and interleaved with oscillators belonging to a second cluster. Conduction velocity between oscillators in separate clusters is such that these oscillators see each other in anti-phase. If conduction velocity is dynamic, it is thus possible that clusters are structurally connected in terms of coupling strength and yet functionally distinct because they are segregated by another structural factor (conduction velocity, see Fig. 11). If both coupling strength and conduction velocity are dynamic, we observed that for a sufficiently large enhancement factor, which determines maximum conduction velocity, a single functional cluster exhibiting zero-mode synchronization emerges. Yet, structural connectivity is characterized by positive values only for neighboring oscillators and negative values between remote oscillators. Conduction velocity counteracts the repellent effects of negative coupling by producing delays of roughly half a period such that negatively coupled oscillator pairs see each other in anti-phase when they are in fact in phase (see Fig. 12). Dynamic conduction velocity thus appears to enable the system to resist the effects of coupling strength and allow for both functional integration of structurally segregated oscillators as well as functional segregation of structurally integrated clusters.

In line with previous work,^{37,55–59} we observe bi- and multistability for nonzero delays, most prominently at boundaries in parameter space. Furthermore, regions of bi/ multistability appear to occur largely as a function of delay (cf. Refs. 37 and 56), either in the form of delay parameter T for scenario I or in the form of the enhancement factor α_v determining the maximum delay for scenarios II and III. In contrast to previous studies that reported bistability of synchronous and incoherent states,^{34,52,53} the circle topology of our network supports bi/multistability between fully synchronous states that differ with respect to their coherent-wave mode of synchronization and single- vs double-cluster-formation, at least as long as either coupling strength or conduction velocity are dynamic. When both coupling strength and conduction velocity are dynamic, we additionally observe bistability between states that can and those that cannot be characterized in terms of standing-wave mode and cluster-formation. These latter states might simply reflect incoherence among oscillators. However, we cannot rule out that they reflect chimera states. This possibility is intriguing in light of previous studies showing that chimera states emerge from a pitchfork bifurcation as a function of coupling delay.^{52,54} The fact that this parameter is itself dynamic in our simulations may give rise to hitherto unobserved behavior (such as chimera states characterized by mixtures of those states described here) and constitute an interesting avenue for further research.

In light of neuroscientific evidence that myelination continues to exhibit adaptive changes even in the adult brain,^{35,60,61} our results highlight the importance of considering this factor in computational models of learning. For instance, our observation that dynamic conduction velocity provides the possibility for synchronization even in the context of fast learning highlights that adaptive myelination may have a useful dampening role to compensate for fast synaptic changes that might otherwise desynchronize neural groups. It may

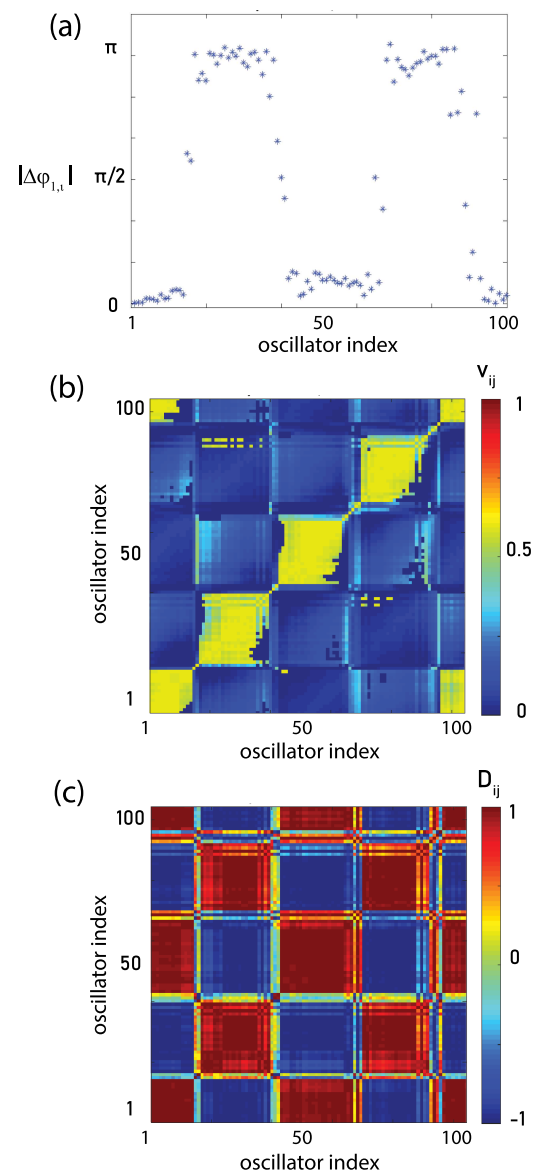


FIG. 11. Dissociation between structural and functional clusters for the state $\{2,d\}$ observed in scenario II. Panel (a) shows phase offsets between every oscillator and the first ($|\Delta\varphi_{1,i}|$). Offsets reflect two anti-phase clusters. Panel (b) shows pairwise conduction velocity reflecting four structural clusters. Panel (c) shows pairwise functional connectivity reflecting two functional clusters.

thus prevent networks in the brain from associating or dissociating too quickly under the influence of experiences. Interestingly, this compensation involves both increases and decreases in conduction velocity, highlighting that simply maximizing conduction speed is not necessarily optimal.³² Furthermore, the compensatory effect of dynamic conduction velocity could be observed in our simulations even when its rate of change is a factor of 10 slower than that of

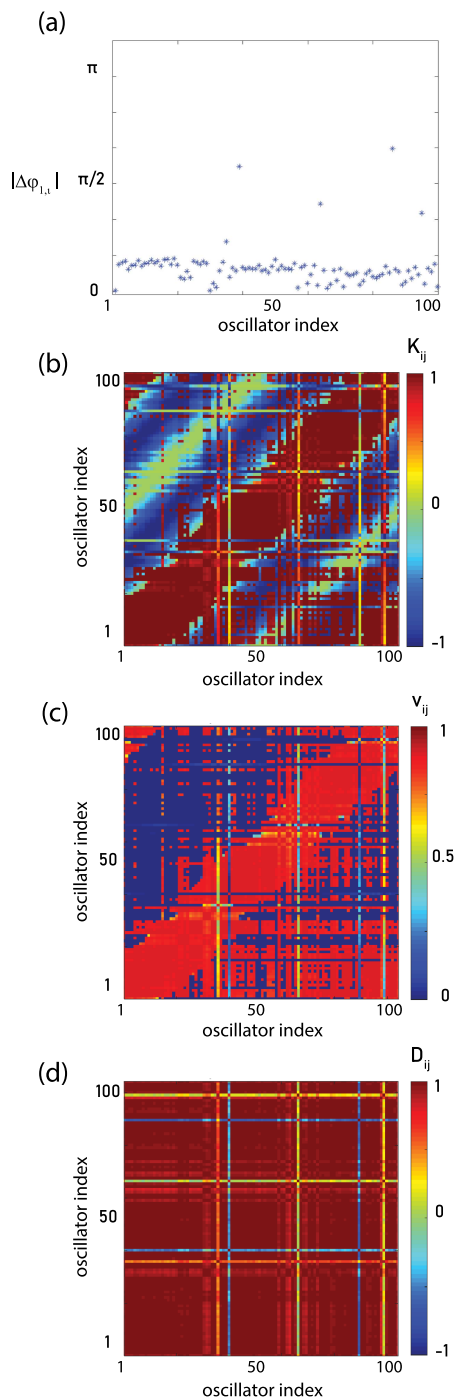


FIG. 12. Dissociation between structural and functional clusters for state $\{0,s\}$ observed in scenario III. Panel (a) shows phase offsets between every oscillator and the first ($|\Delta\phi_{1,i}|$). Offsets reflect a single (global) cluster. Panel (b) shows pairwise structural connectivity reflecting two clusters. Panel (c) shows pairwise conduction velocity reflecting two clusters. Panel (d) shows pairwise functional connectivity reflecting a single cluster.

synaptic strength. This suggests that our findings are relevant for the biologically plausible scenario where myelin related changes lag behind changes in synaptic efficacy, as it may take up to several weeks of daily stimulation of neuronal axons before changes in myelination can be detected.^{62,63} A role of slowly changing myelination in sharpening synchronization during neuronal communication would be in line with several theories in which rhythmic spike synchronization is thought to determine the efficiency of neural communication.^{64–67} Our results call for an investigation of the neurocomputational mechanisms allowing for activity- and experience-dependent modulations of adaptive myelination. Based on observations that white matter structural changes resemble synaptic changes to the extent that they depend on the frequency of neural coactivation,^{32–36,38,61,68} we implemented it as a Hebbian learning process. This is surely an oversimplification given that the control of myelination in adults, while incompletely understood, involves glia-neuronal interactions. We could not consider these here due to the simplicity of our model. Future work is thus needed to develop a more biologically appropriate learning mechanism and embed it in a model incorporating both types of cells. Nevertheless, our approach captures the most essential dynamical aspect of adaptive myelination, namely that conduction velocity of frequently used connections is strengthened while that of rarely used connections is weakened. Other simplifications of our work include the arrangement of oscillators along a circle, arbitrary units of space and time, and the lack of input. However, using these simplifications, we were able to decrease the complexity of computations and the number of parameters in order to plainly identify the influences of synaptic and myelin plasticity on the collective behavior of oscillators. Furthermore, since the system studied here is not intended to address any specific neural processes, our results are sufficiently general to be translated to several spatial and temporal scales. Future research will be necessary to investigate the contribution of realistic network topology as well as of functionally relevant external stimulation.

SUPPLEMENTARY MATERIAL

See the [supplementary material](#) for the overall view of the changes in structural and functional characteristic behavior of the network in relation to the learning parameters.

ACKNOWLEDGMENTS

P.D.W. was supported by an NWO VICI grant (No. 453.04.002). M.S. was funded by the European Union's Horizon 2020 Research and Innovation Program under Grant Agreement No. 737691 (HBP SGA2). M.M. was supported by an NWO VENI grant (No. 451.15.012). This work was supported by the Dutch Province of Limburg.

REFERENCES

- ¹A. Pikovsky, M. Rosenblum, and J. Kurths, *Synchronization: A Universal Concept in Nonlinear Sciences*, Cambridge Nonlinear Science Series (Cambridge University Press, 2001).
- ²H. Haken, *Brain Dynamics: Synchronization and Activity Patterns in Pulse-Coupled Neural Nets with Delays and Noise* (Springer, 2002).
- ³H. F. El-Nashar, Y. Zhang, H. A. Cerdeira, and A. F. Ibiyinka, *Chaos* **13**, 1216 (2003).

- ⁴A. Mörtl, T. Lorenz, and S. Hircze, *PLoS One* **9**, e95195 (2014).
- ⁵P. Kumar, D. K. Verma, and P. Parmananda, *Phys. Lett. A* **381**, 2337 (2017).
- ⁶D. Gonze, S. Bernard, C. Waltermann, A. Kramer, and H. Herzog, *Biophys. J.* **89**, 120 (2005).
- ⁷J. F. Hipp, A. K. Engel, and M. Siegel, *Neuron* **69**, 387 (2011).
- ⁸C. M. Krause, B. Pörn, A. H. Lang, and M. Laine, *Cogn. Brain Res.* **5**, 295 (1997).
- ⁹L. Melloni, C. Molina, M. Pena, D. Torres, W. Singer, and E. Rodriguez, *J. Neurosci.* **27**, 2858 (2007).
- ¹⁰J. Fell, P. Klaver, C. E. Elger, and P. Fries, *Brain Res. Rev.* **42**, 265 (2003).
- ¹¹S. M. Doesburg, A. B. Roggeveen, K. Kitajo, and L. M. Ward, *Cereb. Cortex* **18**, 387 (2008).
- ¹²T. Womelsdorf and P. Fries, *Curr. Opin. Neurobiol.* **17**, 154 (2007).
- ¹³Y. Kazanovich and R. Borisyuk, *Neural Netw.* **87**, 1 (2017).
- ¹⁴O. Burylko, Y. Kazanovich, and R. Borisyuk, *Sci. Rep.* **8**, 416 (2018).
- ¹⁵G. Zouridakis, F. Baluch, I. Stevenson, J. Diaz, and D. Subramanian, in *3rd International IEEE/EMBS Conference on Neural Engineering, Kohala Coast, HI, 2–5 May 2007* (IEEE, 2007), pp. 310–313.
- ¹⁶R. Q. Quiroga, J. Arnhold, and P. Grassberger, *Phys. Rev. E* **61**, 5142 (2000).
- ¹⁷J.-P. Pfister and W. Gerstner, *J. Neurosci.* **26**, 9673 (2006).
- ¹⁸W. Singer, *Annu. Rev. Physiol.* **55**, 349 (1993).
- ¹⁹S. Song, K. D. Miller, and L. F. Abbott, *Nat. Neurosci.* **3**, 919 (2000).
- ²⁰P. Seliger, S. C. Young, and L. S. Tsimring, *Phys. Rev. E* **65**, 041906 (2002).
- ²¹T. Nowotny, V. P. Zhigulin, A. I. Selverston, H. D. I. Abarbanel, and M. I. Rabinovich, *J. Neurosci.* **23**, 9776 (2003).
- ²²R. K. Niyogi and L. Q. English, *Phys. Rev. E* **80**, 066213 (2009).
- ²³L. Timms and L. Q. English, *Phys. Rev. E* **89**, 032906 (2014).
- ²⁴B. Siri, M. Quoy, B. Delord, B. Cessac, and H. Berry, *J. Physiol. Paris* **101**, 136 (2007).
- ²⁵R. D. Traubab, N. Spruston, I. Soltesz, A. Konnerth, M. A. Whittington, and J. G. Jefferys, *Prog. Neurobiol.* **55**, 563 (1998).
- ²⁶D. O. Hebb, *The Organization of Behavior* (Wiley, New York, 1949).
- ²⁷H. Markram, L. H. R. Lübke, M. Frotscher, and B. Sakmann, *Science* **275**, 213 (1997).
- ²⁸Y. L. Maistrenko, B. Lysyansky, C. Hauptmann, O. Burylko, and P. A. Tass, *Phys. Rev. E* **75**, 066207 (2007).
- ²⁹O. V. Popovych, S. Yanchuk, and P. A. Tass, *Sci. Rep.* **3**, 2926 (2013).
- ³⁰D. V. Kasatkin, S. Yanchuk, E. Schöll, and V. I. Nekorkin, *Phys. Rev. E* **96**, 062211 (2017).
- ³¹R. D. Fields, *Science* **344**, 264 (2014).
- ³²R. D. Fields, *Nat. Rev. Neurosci.* **16**, 756 (2015).
- ³³I. A. McKenzie, D. Ohayon, H. Li, J. P. De Faria, B. Emery, K. Tohyama, and W. D. Richardson, *Science* **346**, 318 (2014).
- ³⁴M. Nickel and C. Gu, *Neural Plast.* **2018**, 1 (2018).
- ³⁵J. Scholz, M. C. Klein, T. E. J. Behrens, and H. Johansen-Berg, *Nat. Neurosci.* **12**, 1370 (2009).
- ³⁶D. Purger, E. M. Gibson, and M. Monje, *Neuropharmacology* **110**, 563 (2016).
- ³⁷M. K. S. Yeung and S. H. Strogatz, *Phys. Rev. Lett.* **82**, 648 (1999).
- ³⁸K.-J. Chang, S. A. Redmond, and J. R. Chan, *Nat. Neurosci.* **19**, 190 (2016).
- ³⁹S. Pajevic, P. J. Basser, and A. R. D. Fields, *Neuroscience* **276**, 135 (2014).
- ⁴⁰D. J. Dutta, D. Ho, P. R. Lee, S. Pajevic, O. Bukalo, W. C. Huffman, and H. Wake, *Proc. Natl. Acad. Sci. U. S. A.* **115**, 11832 (2018).
- ⁴¹R. D. Fields, *Science* **330**, 768 (2010).
- ⁴²K. Barrera, P. Chu, J. Abramowitz, R. Steger, R. L. Ramos, and J. C. Brumberg, *Dev. Neurobiol.* **73**, 297 (2013).
- ⁴³R. J. Zatorre, R. D. Fields, and H. Johansen-berg, *Nat. Neurosci.* **15**, 528 (2012).
- ⁴⁴J. A. Acebrón, L. L. Bonilla, C. J. P. Vicente, F. Ritort, and R. Spigler, *Rev. Mod. Phys.* **77**, 137 (2005).
- ⁴⁵G. M. Wittenberg and S. S.-H. Wang, *J. Neurosci.* **26**, 6610 (2006).
- ⁴⁶G. Q. Bi and M. M. Poo, *J. Neurosci.* **18**, 10464 (1998).
- ⁴⁷D. H. Zanette, *Phys. Rev. E* **62**, 3167 (2000).
- ⁴⁸K. Dénes, B. Sándor, and Z. Nédá, *Commun. Nonlinear Sci. Numer. Simul.* **78**, 104868 (2019).
- ⁴⁹M. Schröder, M. Timme, and D. Witthaut, *Chaos* **27**, 073119 (2017).
- ⁵⁰Y. Kuramoto and D. Battogtokh, *Nonlinear Phenom. Complex Syst.* **5**, 380 (2002).
- ⁵¹D. M. Abrams and S. H. Strogatz, *Phys. Rev. Lett.* **93**, 174102 (2004).
- ⁵²T. Kotwal, X. Jiang, and D. M. Abrams, *Phys. Rev. Lett.* **119**, 264101 (2017).
- ⁵³N. Yao, Z.-G. Huang, Y.-C. Lai, and Z.-G. Zheng, *Sci. Rep.* **3**, 3522 (2013).
- ⁵⁴C. R. Laing, *Chaos* **19**, 013113 (2009).
- ⁵⁵Y. Nakamura, F. Tominaga, and T. Munakata, *Phys. Rev. E* **49**, 4849 (1994).
- ⁵⁶H. G. Schuster and P. Wagner, *Prog. Theor. Phys.* **81**, 939 (1989).
- ⁵⁷E. Niebur, H. G. Schuster, and D. M. Kammen, *Phys. Rev. Lett.* **67**, 2753 (1991).
- ⁵⁸E. Montbrío, D. Pazó, and J. Schmidt, *Phys. Rev. E* **74**, 056201 (2006).
- ⁵⁹C. Hauptmann, O. Omel'chenko, O. V. Popovych, Y. Maistrenko, and P. A. Tass, *Phys. Rev. E* **76**, 066209 (2007).
- ⁶⁰E. M. Gibson, D. Purger, C. W. Mount, A. K. Goldstein, G. L. Lin, L. S. Wood, I. Inema, S. E. Miller, G. Bieri, J. B. Zuchero, B. A. Barres, P. J. Woo, H. Vogel, and M. Monje, *Science* **344**, 1252304 (2014).
- ⁶¹C. Sampaio-Baptista, A. A. Khrapitchev, S. Foxley, T. Schlagheck, J. Scholz, S. Jbabdi, G. C. DeLuca, K. L. Miller, A. Taylor, N. Thomas, J. Kleim, N. R. Sibson, D. Bannerman, and H. Johansen-Berg, *J. Neurosci.* **33**, 19499 (2013).
- ⁶²T. Ishibashi, K. A. Dakin, B. Stevens, P. R. Lee, S. V. Kozlov, C. L. Stewart, and R. D. Fields, *Neuron* **49**, 823 (2006).
- ⁶³C. Demerens, B. Stankoff, M. Logak, P. Anglade, B. Allinquant, F. Couraud, B. Zalc, and C. Lubetzki, *Proc. Natl. Acad. Sci. U. S. A.* **93**, 9887 (1996).
- ⁶⁴P. Fries, *Trends Cogn. Sci.* **9**, 474 (2005).
- ⁶⁵P. Fries, *Neuron* **88**, 220 (2015).
- ⁶⁶E. Lowet, B. Gips, M. J. Roberts, P. De Weerd, O. Jensen, and J. van der Eerden, *PLoS Biol.* **16**, e2004132 (2018).
- ⁶⁷O. Jensen and J. E. Lisman, *J. Neurophysiol.* **83**, 2602 (2000).
- ⁶⁸T. Blumenfeld-Katzir, O. Pasternak, M. Dagan, and Y. Assaf, *PLoS One* **6**, e20678 (2011).